THE EUROPEAN PHYSICAL JOURNAL PLUS

Societa Italiana di Fisica (Italian Society of Physics)

ISSN: 2190-5444 (Online); Publisher – Springer

Impact Factor 2.240

Online April 10th 2019

MATHEMATICAL MODELLING OF TWO-FLUID ELECTRO-OSMOTIC PERISTALTIC PUMPING OF AN ELLIS FLUID IN AN AXISYMMETRIC TUBE

N. Ali[1], S. Hussain[1*] , K. Ullah[1] *and* O. Anwar Bég[2]

[1]Department of Mathematics and Statistics, International Islamic University, Islamabad 44000, **Pakistan**.

[2]Department of Aeronautical/Mechanical Engineering, Salford University, Manchester, M54WT, **UK**.

Abstract

This article explores analytically the dynamics of two-fluid electro-osmotic peristaltic flow through a cylindrical tube. The rheology of the fluid in the central core (inner region or core region) is captured through the Ellis equation. The region adjacent to the wall (outer region or peripheral region) is occupied by a Newtonian fluid. The equations governing the flow in each region are modeled by using the appropriate suppositions of long wavelength and low Reynolds number. Closed form expressions for stream function corresponding to each region are obtained and utilized to determine the axial pressure gradient and the interface between the inner and the outer regions. The pumping characteristics, trapping and reflux phenomena are investigated in detail with reference to the Ellis model parameters and the electro-kinetic slip velocity. The present model also generalizes earlier studies from the literature which can be retrieved as special cases. The analysis shows that pressure drop at zero volumetric flow rate is elevated with increasing occlusion parameter. Trapping and reflux phenomena are mitigated with increasing electro-osmotic slip and shear-thinning effects. At larger value of the occlusion parameter an increase in the power-law index reduces the magnitude of the pressure drop. Increasing Ellis rheological parameter reduces the pressure drop over the entire range of occlusion parameters for the case when the peripheral region fluid viscosity exceeds that of the core region fluid. The results obtained may be applicable in the modulation of peristaltic pumping in the efficient operation of various industrial and bio-medical devices.

Keywords: *Peristaltic flow, Ellis fluid, Electro-osmosis, Trapping, Reflux, Biological pumps.*

**Corresponding author*: Email: sadaqatkhan366@gmail.com*

1. Introduction

Peristalsis is an important mechanism of physiological fluid transport in living organs. In this mechanism, the fluid contained in the conduit is transported via the sinusoidal movements of the boundary of the conduit. Many modern bio-medical devices and chemical pumps have been designed by exploiting the peristaltic mechanism. Examples include heart-lung machines, diabetic pumps, waste migration control pumps, roller and finger pumps and pharmacological drug delivery systems. These applications and new emerging ones have mobilized significant activity in theoretical studies of peristaltic fluid dynamics. One of the earliest theoretical models, developed by Shapiro *et al*. [1], approximates the actual situation as the flow in a flexible tube with a sinusoidally deformed boundary. The equation governing the flow was modeled in [1] under creeping flow and long wavelength assumptions. The pumping, trapping and reflux phenomena were discussed in detail. Later studies on this topic can be considered as the extensions of the work of Shapiro *et al.* Several important effects investigated in these extensions include the: non-Newtonian fluid characteristics (rheology) [2 - 6], inertial and streamline curvature effects [7, 8], heat and mass transfer effects [9 - 11], conduit wall elastic effects [12, 13], wall curvature effects [14 - 16], wave profile effect [17, 18]. These studies do throw light on the important aspect of augmentation of peristaltic flow. However, the first systematic study focusing on this aspect was presented later by Chakraborty [19]. The idea presented by Chakraborty was precisely the modulation of peristaltic transport via an electro-kinetic body force. The idea of fluid transport via electroosmotic force has been established for many decades and interesting works in this regard include [20 - 22]. However, Chakraborty [19] was the first to successfully applied electro-osmotics it to peristaltic flows. More recent studies dealing with the application of electro-osmotic methods for transportation of fluid in channel or tube were carried out by Afonso *et al*. [23, 24], Dhinakaran *et al.* [25], Ferras *et al.* [26], Das and Chakraborty [27]. The analysis of Chakraborty [19] was also extended by several researchers. In this regard, Tripathi *et al.* [28] extended Chakraborty's model with the inclusion of a transverse magnetic field for time-depended peristaltic flow. Tripathi *et al.* [29] further expanded the Chakraborty model to consider peristaltic electro-osmotic pumping of water-based nanofluids flow in a complex wavy (micro) channel with Joule heating and buoyancy effects. Prakash and Tripathi [30] discussed the flow of non-Newtonian ionic nanofluid in a tapered peristaltic channel. They utilized constitutive equations of the Williamson viscoelastic model and

obtained linearized solutions via perturbation and MATLAB routine bvp-4c methods. More recently, Goswami *et al.* [31] investigated the effect of electro-osmosis on the two-layered peristaltic flow in a tube with relevance to blood flow in vessels. They characterized the core region fluid by the power-law model. However, a more general constitutive equation can be integrated in the frame work of the model considered by Goswami *et al.* [31]. Therefore, the aim of our work is to complement the analysis of Goswami *et al*. [31] by incorporating the Ellis rheological model in the analysis. The Ellis model is a generalization of the power-law and Bingham (viscoplastic) models. It behaves as a power-law model at *high values of shear stresses* and as the Newtonian model at *low shear stresses*. The constitutive equation of the Bingham model can also be deduced from the constitutive equation of the Ellis model. Therefore, the Ellis model can be considered as a generalization of the power-law, Bingham and Newtonian models and provides a good framework for predicting the rheology of several bio-fluids such as blood, cervical mucus, respiratory mucus, chyme etc. Some important studies pertaining to the use of the Ellis model in modeling and analysis of various flows can be found in [32, 33].

The paper is structured as follows: The geometric model for the flow problem is defined in section 2. The mathematical formulation is developed in section 3 wherein streamline function and velocity are also derived. A parametric study of the impact of rheological, geometric, peristaltic wave and electro-osmotic effects on key flow characteristics (pressure drop etc) is presented in section 4 where all results are visualized graphically and interpreted at length. The key findings from the study are summarized in the conclusions in section 5.

2. Geometric Model of the Physical Problem

We consider a flexible cylindrical tube of un-deformed radius r_0 through which a bio-fluid is flowing due to peristaltic movement of the tube boundary and under the action of an electro-osmotic body force as shown in **Fig. 1**.

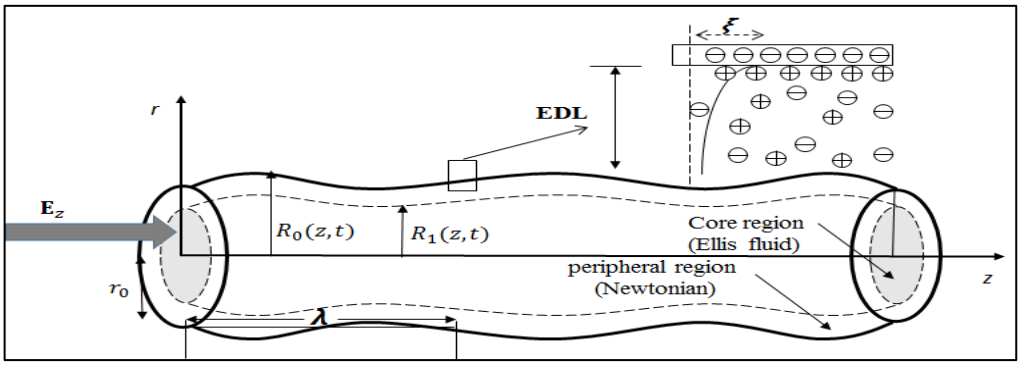

Fig. 1: Geometry of the flow problem.

The region inside the tube is composed of the peripheral and core regions. The fluid in the core region is characterized by the Ellis model whereas the fluid in the peripheral region obeys the Newtonian constitutive law. The negatively charged wall of the tube attracts opposite ions in the polar fluid forming a layer of positively charged fluid near the wall and at the same time repels the counter-ions. The thin layer of immobile counter-ions covering the inner side of the wall is known as the *Stern layer*. Below the Stern layer, a thicker layer of moving counter-ions develops. The combination of the Stern layer and the thicker layer is known as the electric double layer (EDL). The electro-kinetic body force emerges by connecting the system to an external applied electric field. The resulting multi-physical fluid dynamic problem encompasses the computation of the flow field developed by the combined effects of the wall movement and the electro-kinetic body force.

3. Mathematical Model

The vector form of the momentum equation for the flow under consideration (Fig. 1) is given by:

$$\rho_f \left(\frac{D\mathbf{u}}{Dt}\right) = -\nabla p + \nabla.\mathbf{S} + \mathbf{F}_{EK}, \tag{1}$$

where ρ_f is the density of the fluid, $\mathbf{S}$ the extra stress tensor, p the pressure and, $\mathbf{F}_{EK}$ is the electro-kinetic body force. The continuity equation is given by:

$$\left(\frac{\partial \rho_f}{\partial t}\right) + \nabla\left(\rho_f \mathbf{u}\right) = 0. \tag{2}$$

The extra stress tensor $\mathbf{S}$ is defined differently for both the core (Ellis fluid) and the peripheral (Newtonian) regions:

$$\mathbf{S} = \begin{cases} \mu_c(\gamma)\,\dot{\boldsymbol{\gamma}}, & 0 \le r < R_1(z,t), \\ \mu_N\,\dot{\boldsymbol{\gamma}}, & R_1 \le r < R_0(z,t), \end{cases} \tag{3}$$

where R_1 is the expression for the interface between the core and peripheral regions. Since, the core region is characterized by the Ellis model, therefore the appropriate rheological relation is:

$$\mu_c(\gamma) = \frac{\mu_0}{1+\left(\frac{\pi_s}{\tau^2_0}\right)^{\alpha-1}}, \tag{4}$$

Here μ_0 represents the zero-shear rate viscosity, π_s denotes the second invariant stress tensor $\dot{\boldsymbol{\gamma}}$, α is the power-law index and quantifies shear-thinning behavior $(\alpha > 1)$, τ_0 is the shear stress at which the apparent viscosity becomes $\mu_0/2$, $\dot{\boldsymbol{\gamma}}$ $(= (1/2)\{\nabla\mathbf{u} - (\nabla\mathbf{u})^T\})$ is the strain-rate tensor and μ_N is the viscosity of Newtonian fluid in the peripheral region. For axisymmetric incompressible flow in the tube, it is appropriate to define the velocity vector as follows:

$$\mathbf{u} = [u(r,z,t), 0, w(r,z,t)]. \tag{5}$$

In view of above velocity field, the basic equations (1) and (2) the presence of the electro-kinetic force applied in the axial direction yield

$$\frac{1}{r}\frac{\partial(ru)}{\partial r} + \frac{\partial w}{\partial z} = 0, \tag{6}$$

$$\rho_f\left(\frac{\partial u}{\partial t} + u\frac{\partial u}{\partial r} + w\frac{\partial u}{\partial z}\right) = -\frac{\partial p}{\partial r} + \left[\frac{1}{r}\frac{\partial(rS_{rr})}{\partial r} + \frac{\partial S_{rz}}{\partial z} - \frac{S_{\theta\theta}}{r}\right], \tag{7}$$

$$\rho_f\left(\frac{\partial w}{\partial t} + u\frac{\partial w}{\partial r} + w\frac{\partial w}{\partial z}\right) = -\frac{\partial p}{\partial z} + \left[\frac{1}{r}\frac{\partial(rS_{rz})}{\partial r} + \frac{\partial S_{zz}}{\partial z}\right] + F_{EK}. \tag{8}$$

It is noteworthy that:

$$(\rho_f, u, w) = \begin{cases} \rho_c, u_c, w_c \\ \rho_N, u_N, w_N \end{cases} \tag{9}$$

where the subscript *c* stands for the core region whereas *N* designates the peripheral region. When the external electric field E_z is applied, the liquid undergoes a body force which takes the form [34]:

$$F_{EK} = \rho_e E_z\ , \tag{10}$$

where ρ_e is the total ionic charge concentration which is considered as the sum of ρ_{eN} and ρ_{ec}, the ionic charge concentrations corresponding to the peripheral and the core regions, respectively. The motion of the tube is assumed to be a periodic peristaltic wave motion with wave speed U and the wavelength λ. The radius of the tube R_0 is a function of $(z - Ut)$ in the fixed frame. However, switching the analysis from the fixed frame (r, z) to the moving frame $(\bar{r}, \bar{z})$ it can be made a function of $\bar{z}$ alone. The conversion between fixed frames to wave frame is achieved via the following transformations:

$$\bar{z} \to z - Ut, \bar{r} \to r, \bar{u} \to u, \bar{w} \to w - U, \bar{p} \to p. \tag{11}$$

By using these transformations, the momentum and continuity equations in the moving frame of reference reduce to the following equations:

$$\frac{1}{\bar{r}}\frac{\partial(\bar{r}\,\bar{u})}{\partial\bar{r}} + \frac{\partial\bar{w}}{\partial\bar{z}} = 0, \tag{12}$$

$$\rho_f\left(\bar{u}\frac{\partial\bar{u}}{\partial\bar{r}} + \bar{w}\frac{\partial\bar{u}}{\partial\bar{z}}\right) = -\frac{\partial\bar{p}}{\partial\bar{r}} + \left[\frac{1}{\bar{r}}\frac{\partial(\bar{r}\,\bar{S}_{\bar{r}\bar{r}})}{\partial\bar{r}} + \frac{\partial\bar{S}_{\bar{r}\bar{z}}}{\partial\bar{z}} - \frac{\bar{S}_{\bar{\theta}\,\bar{\theta}}}{\bar{r}}\right], \tag{13}$$

$$\rho_f\left(\bar{u}\frac{\partial\bar{w}}{\partial\bar{r}} + \bar{w}\frac{\partial\bar{w}}{\partial\bar{z}}\right) = -\frac{\partial\bar{p}}{\partial\bar{z}} + \left[\frac{1}{\bar{r}}\frac{\partial(\bar{r}\,\bar{S}_{\bar{r}\bar{r}})}{\partial\bar{r}} + \frac{\partial\bar{S}_{\bar{r}\bar{z}}}{\partial\bar{z}} - \frac{\bar{S}_{\bar{\theta}\,\bar{\theta}}}{\bar{r}}\right], \tag{14}$$

where $\bar{\mathbf{S}}$ is the stress tensor in the moving frame of reference. Next the following dimensionless variables are invoked as defined below [31]

$$r = \frac{\bar{r}}{r_0},\ z = \frac{\delta\,\bar{z}}{r_0}\,, u = \frac{\bar{u}}{(\delta\,U)},\quad t = \frac{\delta\,U}{r_0}t,\ p = \frac{\delta\,r_0}{\mu_c\,U}\bar{p}\,, Re = \frac{Ur_0}{\mu_0}\,,$$

$$S = \frac{\mu_0\,U}{r_0}, \beta = \frac{U}{r_0\tau_0^{\,2}}\,, \text{ and } F_{EK} = \frac{-F\,{r_0}^2\,\epsilon_K}{\epsilon_N\xi E_z}, \tag{15}$$

Eqns. (12) - (15) in the *core region* now assume the non-dimensional form:

$$\frac{1}{r}\frac{\partial(ru_c)}{\partial r} + \frac{\partial w_c}{\partial z} = 0, \tag{16}$$

$$\delta^2\left[\delta Re\left(u_c\frac{\partial u_c}{\partial r} + w_c\frac{\partial u_c}{\partial z}\right)\right] = -\frac{\partial p}{\partial r} + \delta\left[\left(\frac{1}{r}\frac{\partial(r\,S_{rr})}{\partial r} + \frac{\delta\partial S_{rz}}{\partial z}\right) - \frac{S_{\theta\theta}}{r}\right], \tag{17}$$

$$\delta^2\left[\delta Re\left(u_c\frac{\partial w_c}{\partial r} + w_c\frac{\partial w_c}{\partial z}\right)\right] = -\frac{\partial p}{\partial z} + \left[\left(\frac{1}{r}\frac{\partial(r\,S_{rz})}{\partial r}\right)\right] + \frac{\epsilon_N\mu_N\,U_E}{\epsilon_c\mu_c}\rho_{ec}, \tag{18}$$

Here the following definitions apply:

$$S_{rr} = \frac{2\delta\frac{\partial u_c}{\partial r}}{1+(\beta\chi)^{\alpha-1}}\,, S_{rz} = \frac{2\left(\delta^2\frac{\partial u_c}{\partial r}+\frac{\partial w_c}{\partial r}\right)}{1+(\beta\chi)^{\alpha-1}}\,, S_{\theta\theta} = \frac{\delta\frac{u_c}{r}}{1+(\beta\chi)^{\alpha-1}}\,, S_{zz} = \frac{2\delta\frac{\partial w_c}{\partial z}}{1+(\beta\chi)^{\alpha-1}}\,,$$

$$\chi = \left[(1/2)\left({S_{rr}}^2 + {S_{\theta\theta}}^2 + {S_{zz}}^2 + 2\,{S_{rz}}^2\right)\right]^{1/2} \tag{19}$$

Furthermore ϵ_N is the dielectric constant in the outer region, ϵ_c is the dielectric constant in the inner region and $U_E = -\epsilon_N\xi E_z/\mu_N\,U$ is the electrokinetic slip velocity.

Similarly, in the *peripheral region* the relevant normalized equations take the form:

$$\frac{1}{r}\frac{\partial(ru_N)}{\partial r}+\frac{\partial w_N}{\partial z}=0, \tag{20}$$

$$\delta^2\left[\delta Re\left(u_N\frac{\partial u_N}{\partial r}+w_N\frac{\partial u_N}{\partial z}\right)\right]=-\frac{\partial p}{\partial r}+\delta\left[\left(\frac{1}{r}\frac{\partial(r\,S_{rr})}{\partial r}+\frac{\delta\partial S_{rz}}{\partial z}\right)-\frac{S_{\theta\theta}}{r}\right], \tag{21}$$

$$\delta^2\left[\delta Re\left(u_N\frac{\partial u_N}{\partial r}+w_N\frac{\partial w_N}{\partial z}\right)\right]=-\frac{\partial p}{\partial z}+\left[\left(\frac{1}{r}\frac{\partial(r\,S_{rz})}{\partial r}\right)\right]+\frac{\epsilon_N\mu_N\,U_E}{\epsilon_c\mu_c}\rho_{ec}, \tag{22}$$

Where:

$$S_{rr}=2\mu_N\,\delta\,\frac{\partial u_N}{\partial r},\ S_{rz}=\mu_N\left(\delta^2\frac{\partial u_N}{\partial z}+\frac{\partial w_N}{\partial r}\right),$$

$$S_{\theta\theta}=2\mu_N\,\delta\,\frac{u_N}{r},\ S_{zz}=2\mu_N\,\delta\,\frac{\partial w_N}{\partial z}, \tag{23}$$

By using the approximations of long wavelength ($\delta \ll 1$) and low Reynolds number (Re) the momentum equations and the stress components in the core and peripheral regions reduce to:

Core region:

$$0=-\frac{\partial p}{\partial z}+\left[\left(\frac{1}{r}\frac{\partial(r\,S_{rz})}{\partial r}\right)\right]+U_E\,\frac{\mu_r}{\epsilon_r}\rho_{ec}, \tag{24a}$$

$$0=\frac{\partial p}{\partial r}, \tag{24b}$$

$$S_{rr}=S_{\theta\theta}=S_{zz}=0,\ S_{rz}=\frac{\left(\frac{\partial w}{\partial r}\right)}{1+(\beta S_{rz})^{\alpha-1}}. \tag{24c}$$

Peripheral region:

$$0=-\frac{\partial p}{\partial z}+\mu_r\,\frac{1}{r}\left(\frac{\partial(r\,S_{rz})}{\partial r}\right)+U_E\,\mu_r\,\rho_{eN}\quad\text{where}\quad\mu_r=\frac{\mu_N}{\mu_0} \tag{25a}$$

$$0=\frac{\partial p}{\partial r}, \tag{25b}$$

$$S_{rr}=S_{\theta\theta}=S_{zz}=0,\ S_{rz}=\left(\frac{\partial w}{\partial r}\right). \tag{25c}$$

The boundary conditions are:

$$\frac{\partial u_c}{\partial r} = 0, at\ \ r = 0; \quad \text{(symmetry at the center-line)} \tag{26a}$$

$$w_c = w_N \text{ and } (S_{rz})_N = (S_{rz})_c \text{ at } \ r = R_1;$$

(Continuity of velocity and stress at the interface) (26b)

$$w_N = -1 \text{ at } r = R_0; \text{ (no-slip condition at the wall).} \tag{26c}$$

Following Goswami *et al.* [31], we drop the electrokinetic body force terms from momentum equations (25a-c) and (26a-c) along with suitable modification of the no-slip boundary condition at the wall. In this way, the governing equations and boundary condition take the form:

Core region:

$$0 = -\frac{\partial p}{\partial z} + \left[\left(\frac{1}{r}\frac{\partial (r\, S_{rz})}{\partial r}\right)\right], \tag{27a}$$

$$0 = \frac{\partial p}{\partial r}, \tag{27b}$$

$$S_{rr} = S_{\theta\theta} = S_{zz} = 0,\ S_{rz} = \frac{\left(\frac{\partial w}{\partial r}\right)}{1+(\beta S_{rz})^{\alpha-1}}, \tag{27c}$$

$$\frac{\partial u_c}{\partial r} = 0, at\ \ r = 0. \tag{27d}$$

Peripheral region:

$$0 = -\frac{\partial p}{\partial z} + \mu_r \frac{1}{r}\left(\frac{\partial (r\, S_{rz})}{\partial r}\right), \tag{28a}$$

$$0 = \frac{\partial p}{\partial r}, \tag{28b}$$

$$S_{rr} = S_{\theta\theta} = S_{zz} = 0,\ S_{rz} = \left(\frac{\partial w}{\partial r}\right), \tag{28c}$$

$$\frac{\partial u_c}{\partial r} = 0, at\ \ r = 0, \tag{28d}$$

$$w_N = U_E\ - 1, at\ \ r = R_0. \tag{28e}$$

3.1. Velocity components in term of stream function

The velocity components in term of stream function are defined by the Cauchy-Riemann equations:

$$u = -\frac{\partial \hat{\psi}}{\partial z}, w = -\frac{1}{r}\frac{\partial \hat{\psi}}{\partial r}, \tag{29}$$

Here $\hat{\psi}$ is the stream function in the *moving* frame of reference and is related to its counterpart in the *fixed* frame via the relation $\psi = \hat{\psi} - r^2/2$. Now introducing the stream function, the momentum equations in the core and peripheral regions become:

$$\frac{\partial}{\partial r}\left(\frac{1}{r}\frac{\partial \psi}{\partial r}\right) = \frac{r}{2}\frac{\partial p}{\partial z} + \frac{(\beta)^{\alpha-1}}{(2)^{\alpha}}\left|\frac{\partial p}{\partial r}\right|^{\alpha-1}\frac{\partial p}{\partial r}r^{\alpha}, \quad 0 \le r \le R_1, \tag{30}$$

$$0 = -\frac{\partial p}{\partial z} + \frac{1}{r}\frac{\partial}{\partial r}\left[\left(r\mu_r \frac{\partial}{\partial r}\left(\frac{1}{r}\frac{\partial \psi}{\partial r}\right)\right)\right], \quad R_1 \le r \le R_0. \tag{31}$$

The associated boundary conditions are:

$$\psi(0) = 0, \left.\frac{\partial}{\partial r}\left(\frac{1}{r}\frac{\partial \psi}{\partial r}\right)\right|_{r=0} = 0, \tag{32}$$

$$\psi(R_0) = \frac{q}{2}, \frac{\partial \psi}{\partial r} = (U_E - 1)R_0, \tag{33}$$

$$\psi(R_1) = \frac{q_1}{2}, \tag{34}$$

Here μ_r is the viscosity ratio, q_1, q are the volumetric flow rates through the inner and outer cross-sections of the tube, respectively. Now, integrating the Eqns. (30) and (31) subject to the boundary condition (32) and (33), we arrive at the following expressions for stream function in terms of R_1 for both *core* and *peripheral* regions:

$$\psi = \frac{r^2}{2}\left\{(U_E - 1) + \frac{(\beta)^{\alpha-1}}{(2)^{\alpha}}\left|\frac{\partial p}{\partial z}\right|^{\alpha-1}\frac{\partial p}{\partial z}\left[\frac{2\,r^{\alpha+1}}{(\alpha+1)(\alpha+3)} - \frac{{R_1}^{\alpha+1}}{(\alpha+1)}\right] + \frac{1}{16}\frac{\partial p}{\partial z}\left\{r^2 - 2{R_1}^2\right\} + \right.$$

$$\left.\frac{1}{4\mu_r}\frac{\partial p}{\partial z}\left\{{R_1}^2 - {R_0}^2\right\}\right\}, 0 \le r < R_1, \tag{35}$$

$$\psi = \frac{r^2}{2}(U_E - 1) + \left(\frac{q}{2} - (U_E - 1)\frac{{R_0}^2}{2}\right) + \frac{1}{4\mu_r}\frac{\partial p}{\partial z}\left(r^2 - {R_0}^2\right)^2, R_1 \le r \le R_0. \tag{36}$$

From the above expressions, *axial velocity* emerges as:

$$w(r,z)=\begin{cases}(U_E-1)+\frac{(\beta)^{\alpha-1}}{(2)^{\alpha}}\left|\frac{\partial p}{\partial z}\right|^{\alpha-1}\frac{\partial p}{\partial z}\left[\frac{2\,r^{\alpha+1}}{(\alpha+1)(\alpha+3)}-\frac{{R_1}^{\alpha+1}}{(\alpha+1)}\right]+\frac{1}{16}\frac{\partial p}{\partial z}\{r^2-2{R_1}^2\} \\ \quad+\frac{1}{4\mu_r}\frac{\partial p}{\partial z}\{{R_1}^2-{R_0}^2\},\quad 0\le r<R_1, \\ (U_E-1)+\frac{1}{4\mu_r}\frac{\partial p}{\partial z}\left(r^2-{R_0}^2\right),\ R_1\le r\le R_0.\end{cases} \tag{37}$$

For the subsequent analysis, it is assumed that the shape of the outer boundary can be described by the following expression:

$$R_0(z)=1+\phi_{oc}\sin(2\pi z), \tag{38}$$

where ϕ_{oc} represents the dimensionless occlusion parameter. It is important to point that the solution to the considered problem is still not complete due to the unknowns R_1 and $\partial p/\partial z$ appearing in the expressions (35) and (36). To obtain these unknowns, the following semi-analytical approach is deployed [31]. Using the condition (34), we get:

$$\frac{q_1}{2}=\frac{{R_1}^2}{2}(U_E-1)+\left(\frac{q}{2}-(U_E-1)\frac{{R_0}^2}{2}\right)+\frac{1}{16\mu_r}\frac{\partial p}{\partial z}\left({R_1}^2-{R_0}^2\right)^2, \tag{39}$$

Here q_1 is another constant to be determined. To eliminate q_1 we set $R_0=1$ and $R_1=k$ at $z=0$ in the above equation which yields the following:

$$\frac{q_1}{2}=\frac{k^2}{2}(U_E-1)+\left(\frac{q}{2}-(U_E-1)\frac{1}{2}\right)+\frac{1}{16\mu_r}P_0(k^2-1)^2. \tag{40}$$

Eliminating q_1 between (39) and (40) results in the following equation:

$$\frac{k^2}{2}(U_E-1)+\left(\frac{q}{2}-(U_E-1)\frac{1}{2}\right)+\frac{1}{16\mu_r}P_0(k^2-1)^2=\frac{{R_1}^2}{2}(U_E-1)$$

$$+\left(\frac{q}{2}-(U_E-1)\frac{{R_0}^2}{2}\right)+\frac{1}{16\mu_r}\frac{\partial p}{\partial z}\left({R_1}^2-{R_0}^2\right)^2, \tag{41}$$

where k is the inner layer thickness measured at $z=0$ from the boundary wall and $P_0=(\partial p/\partial z)|_{z=0}$. Thus we have replaced q_1 with another unknown P_0. In this way, there are three unknown to be determined to be able to close the solution i.e., P_0, R_1 and $\partial p/\partial z$. However, there is only one condition available i.e. Eqn. (40). The other two conditions can be furnished as follows. Since the stream function given by the Eqns. (35) and (36) must be same at the interface, therefore it follows that:

$$\frac{(\beta)^{\alpha-1}}{(2)^{\alpha+1}}\frac{\partial p}{\partial z}\left|\frac{\partial p}{\partial z}\right|^{\alpha-1}\frac{{R_1}^{\alpha+3}}{(\alpha+3)}+\frac{1}{16\mu_r}\frac{\partial p}{\partial z}\left({R_0}^4-{R_1}^4\right)+\frac{q}{2}-(U_E-1)\frac{{R_0}^2}{2}+\frac{{R_1}^4}{16}\frac{\partial p}{\partial z}=0. \quad (42)$$

Proceeding with the analysis, the following equation is produced:

$$\frac{(\beta)^{\alpha-1}}{(2)^{\alpha+1}}P_0|P_0|^{\alpha-1}\frac{k^{\alpha+3}}{(\alpha+3)}+\frac{P_0}{16\mu_r}\frac{\partial p}{\partial z}(1-k^4)+\frac{q}{2}-(U_E-1)\frac{1}{2}+\frac{k^4}{16}P_0=0. \quad (43)$$

Effectively Eqns. (41) - (43) can be solved numerically to obtain the values of P_0, R_1 and $\partial p/\partial z$ at each axial position z. The bisection method is used for the computations. This process yields closed form expressions for stream function at each axial position z.

4. Graphical Results and Interpretation

4.1. The interface region

The numerical procedure based on the bisection method is implemented in the symbolic software **Mathematica 8.1** to compute the values of P_0, R_1 and $\partial p/\partial z$ corresponding to each axial position z. The plots of interface R_1 against z for different values of μ_r, α, U_E and β are displayed in **Figs. 2 and 3**. It is important to remember that α and β are the material (rheological) parameters associated with the core fluid Ellis model whereas U_E is the parameter arising from the inclusion of the electro-osmotic effects. Fig. 2 illustrates the variations in the interface R_1 with respect to the parameter μ_r which is the ratio between the viscosities of the outer and inner regions.

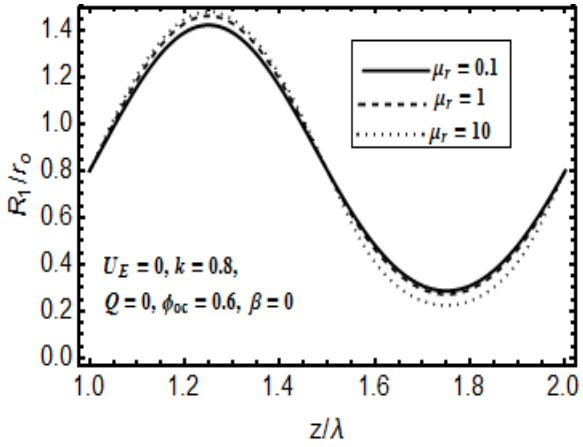

Fig. 2 The behavior of the interface for different values of viscosity ratio μ_r.

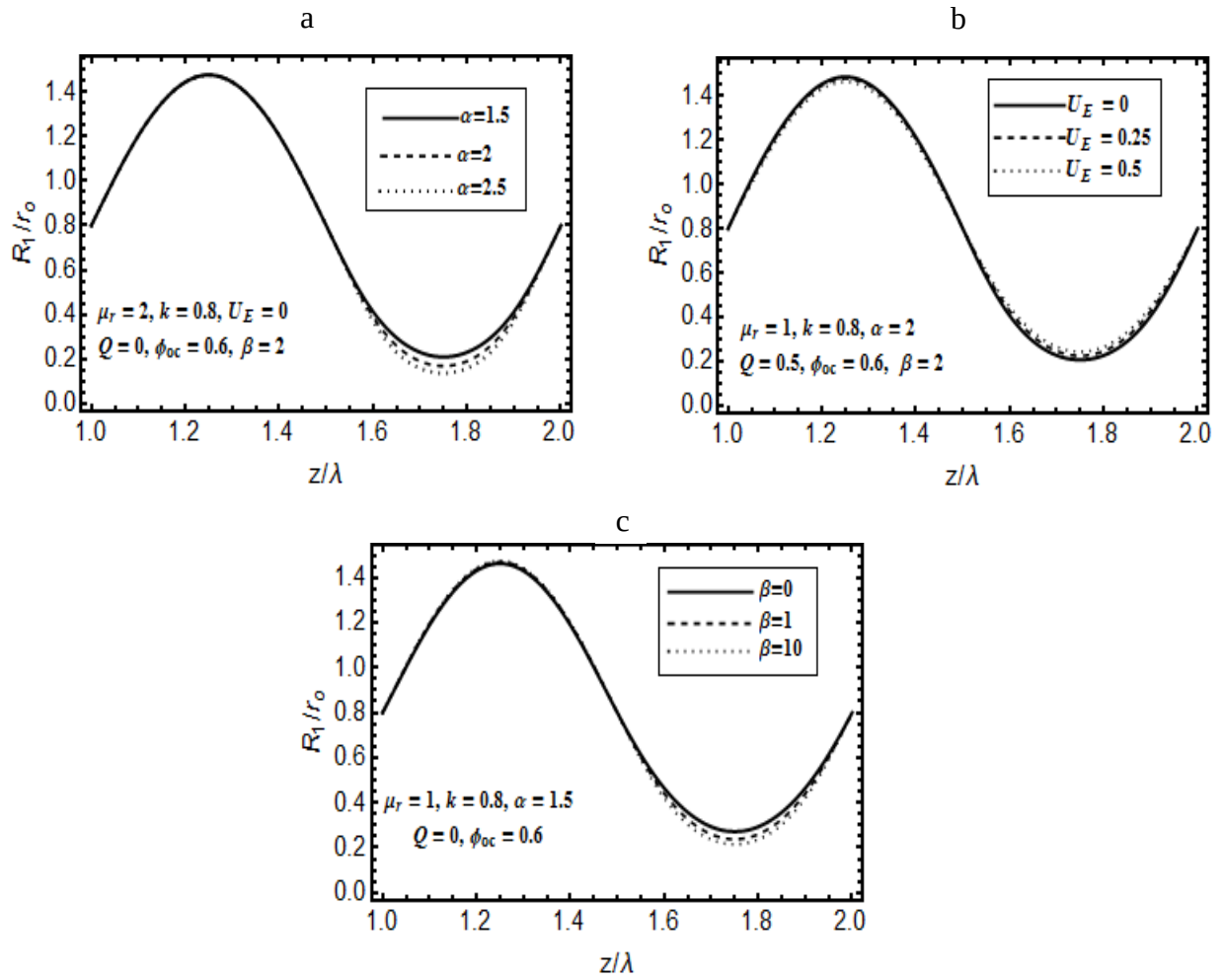

Fig. 3. The variations in interface with respect to Ellis model parameter $\boldsymbol{\alpha}$ and $\boldsymbol{\beta}$ and the electrokinetic parameter $\boldsymbol{U_E}$

It is observed that interface curve corresponding to $\mu_r = 1$ lies in between the corresponding curves for $\mu_r = 0.1$ and $\mu_r = 10$. In fact these curves depict the position of the interface for three situations i.e., $\mu_r < 1$, $\mu_r = 1$ and $\mu_r > 1$. Generally, during the flow the fluid under the crest region will experience a vertical normal force whereas the fluid in the trough region is subjected to a vertically downward force. When $\mu_r < 1$ i.e., the viscosity of the inner core exceeds the viscosity of the outer region, the fluid in the peripheral region under the wave crest will undergo a reduced vertical force in the upward direction and hence stay below the interface level for $\mu_r = 1$. At the same time, the fluid in the outer region under the wave trough will also feel a *reduced force in downward direction* and hence stay above the interface level for $\mu_r = 1$. However, a reverse trend is observed when $\mu_r > 1$. The slight shifting of the fluid in the outer region in both the crest and trough regions is of the same magnitude. However, this is not the situation when the variation is observed with respect to the other parameters such as U_E, β and α. The couple type force

arrangement experienced by the peripheral fluid in the crest and trough region breaks when the core region fluid is assumed to be non-Newtonian. This is attributable to the deformation-dependent viscosity of the non-Newtonian liquid. In the crest region, the normal force acting in the upward direction is least affected with an elevation in either α, U_E and β. Significant changes in the magnitude of normal force are *only observed* in the wave trough region. Therefore, the interface in the trough region is displaced downward with increasing α and β whereas it is displaced upward with increasing U_E .

4.2. Pressure and Volume Flux Variation

The axial pressure gradient $\partial p/\partial z$ in the tube can be computed from the following equation:

$$\frac{\partial p}{\partial z} = \frac{16\mu_r}{\left({R_1}^2 - {R_0}^2\right)^2}\left\{\frac{1}{2}(U_E - 1)\left(k^2 - {R_1}^2 + {R_0}^2\right) + \frac{1}{16\mu_r}P_0(k^2 - 1)^2\right\}. \quad (44)$$

The *pressure rise over one wavelength* is obtained by integrating the above expression from the limits 0 to λ as follows:

$$\Delta P = 16\mu_r \int_0^{\lambda}\left\{\frac{\frac{1}{2}(U_E - 1)\left(k^2 - {R_1}^2 + {R_0}^2\right) + \frac{1}{16\mu_r}P_0\left(k^2 - 1\right)^2}{\left({R_1}^2 - {R_0}^2\right)^2}\right\}dz. \quad (45)$$

The *volume flux in the moving frame* q is related to its counterpart Q_S in the fixed frame of references via the relation:

$$Q_S = 2\int_0^{R_0}(W + 1)\, r\, dr = q + {R_0}^2. \quad (46)$$

Averaging over a complete time-period yields:

$$Q = \frac{1}{T_P}Q_S\, dt = q + \left(1 + \frac{\phi^2}{2}\right), \quad (47)$$

where $T_P = \lambda/U$ is a complete time-period.

The integration in Eqn. (45) is performed numerically and the results computed which illustrate the variations in pressure rise per wavelength *at zero volumetric flow rate* $\Delta P_o = \Delta P|_{Q=0}$ against the occlusion parameter ϕ_{oc} are displayed in **Figs. 4**. This figure infact provides the estimate of dimensionless pressure rise resulting from the peristaltic motion of the wall.

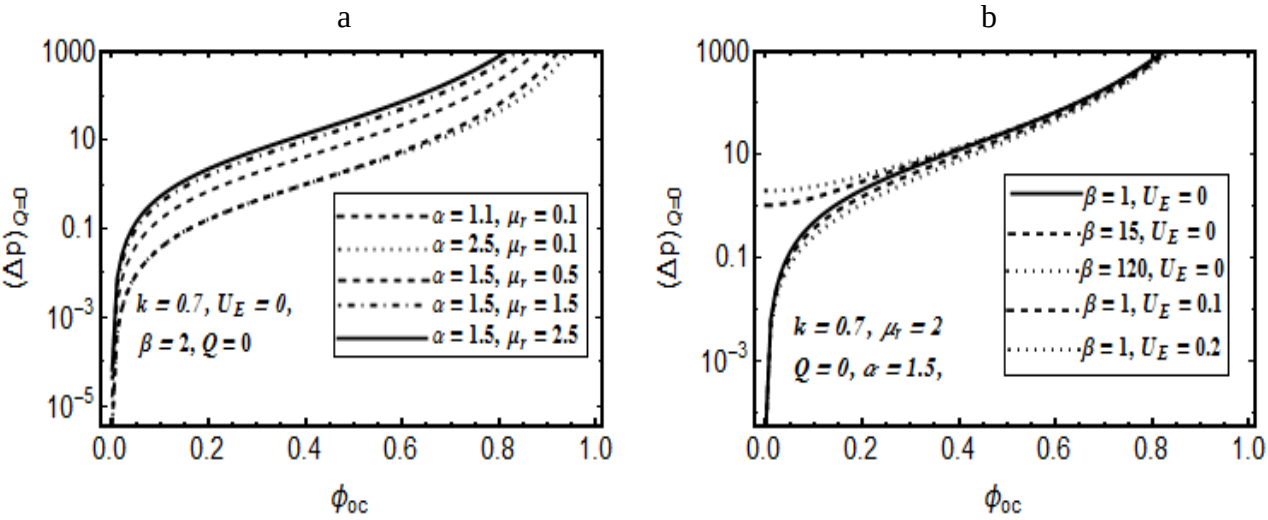

Fig. 4. The pumping characteristics (a) for different values of viscosity ratio and power-law index $\boldsymbol{\alpha}$ and (b) for different values of Ellis parameter $\boldsymbol{\beta}$ and electro-kinetic slip velocity $\boldsymbol{U_E}$.

Fig. 4a shows the results for the case when core region fluid is characterized by the Ellis model. This figure also highlights the influence of viscosity ratio on ΔP_0. Here the effects of electro-osmotic slip are not considered i.e., $U_E = 0$. It is observed that pressure drop at zero volumetric flow rate *increases with increasing occlusion parameter*. A much greater pressure drop is required to maintain zero flow rate when the *core region fluid is less viscous than the peripheral region fluid* in comparison to the scenario where the *outer region is less viscous than the inner region fluid*. Further, the effects of the viscosity ratio are more pronounced in comparison to the effects of the power-law index, α. Infact, the effects of α are only realized at larger values of the occlusion parameter ϕ_{oc}. At larger values of the occlusion parameter an increase in the power-law index reduces the magnitude of ΔP_0. The parameter α is in fact a measure of the *shear-thinning* nature of the fluid in the core region. Larger values of α correspond to the case of fluid with pronounced share-thinning effects i.e., fluid with a significantly reduced apparent viscosity. Therefore, the depletion in pressure associated with increasing α at large occlusion is attributable to the decreased apparent viscosity of the fluid in the inner region. The effects of electro-osmotic slip velocity on ΔP_0 are shown in Fig. 4b. Here it is evident that the presence of electro-osmotic slip velocity reduces the pressure drop only for intermediate values of the occlusion parameter. As the occlusion parameter approaches unity, the reduction is almost negligible. The effects of the Ellis parameter β on ΔP_0 are displayed in Fig. 4b. It is observed that the role of the parameter β is to decrease the

pressure drop over the whole considered range of the occlusion parameter ϕ_{oc}, when the peripheral region fluid is more viscous than the core region fluid. In contrast, when the core region fluid is more viscous than the peripheral region fluid the reduction in pressure drop with increasing β is only realizable at larger values of the occlusion parameter.

4.3. Trapping phenomena

The streamline plots showing trapping inside the core and peripheral regions are displayed in **Figs. (6) – (8)**. A detailed explanation regarding the development of trapped bolus in the flow domain is provided by Goswami *et al*. [31]. According to [31], trapping is strongly dependent upon the *bulk momentum* of the flow. The greater the momentum of the fluid, the lower the probability of fluid particles being trapped in zones of re-circulation. **Fig. 5** illustrates the effects of electro-osmotic slip velocity on the trapped bolus for the case when the inner core is less viscous than the peripheral region. It is observed that the trapped bolus, *regardless of its position*, reduces in size and finally vanishes with increasing the electro-osmotic slip velocity. For the case when viscosity of the inner core exceeds the viscosity of the peripheral region, the trapped bolus appearing either in the core or peripheral regions is *smaller* than its counterpart for the previous case. Fig. 8 shows that the effect of viscosity ratio on the trapped bolus is same as that observed for electro-osmotic slip velocity. Similarly, it is inferred from Fig. 6 that the fluid power-law index α exerts a similar effect on the trapped bolus as that observed for viscosity the ratio and the electro-osmotic slip velocity. In contrast, Fig. 7 reveals that the trapped bolus either in the core or peripheral regions increases in size with an increase in the Ellis model parameter β. However, the increase in the bolus size with increasing Ellis model parameter β is not indefinite i.e., the size of the trapped bolus increases with initial increase in β upto a certain value and thereafter it becomes independent of β. For $\mu_r = 1$, the constancy in the size of the trapped bolus is observed at values of β that are significantly larger than their counterparts for $\mu_r > 1$.

It is also of great use to determine the parametric ranges in which the trapping phenomenon occurs. In this regard, we have presented plots of $Q/Q_{\Delta p=0}$ against the occlusion parameter for several values of the key parameters such as electro-kinetic slip velocity, viscosity ratio and material parameters of the Ellis model in Figs. 9(a - d). In fact, for each ϕ_{oc} there exists a unique value of $Q/Q_{\Delta p=0}$ and vice-versa.

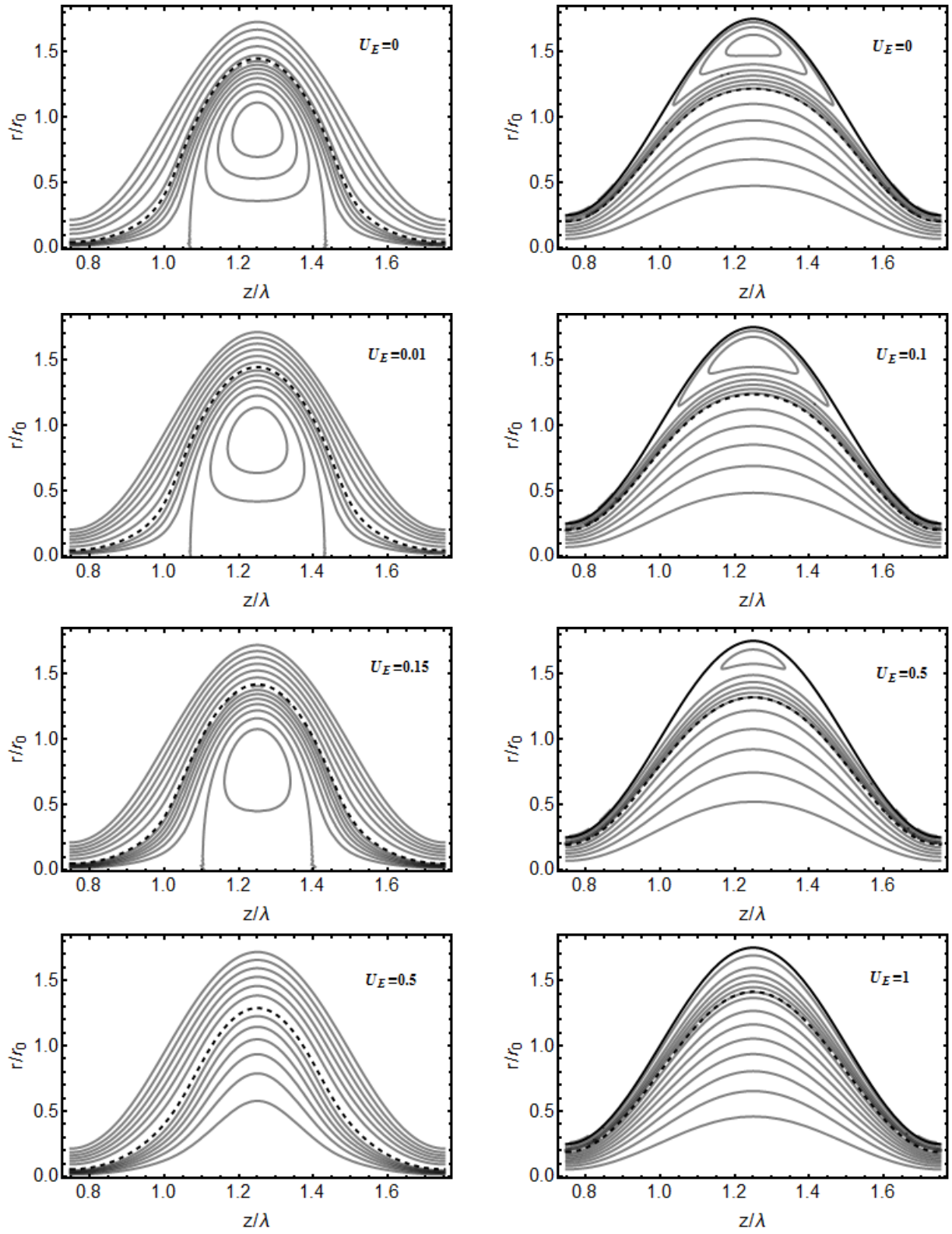

Fig. 5. Streamline plots showing trapping inside the core region (left panels) with other parameters $Q = 0$, *k=0.4*, $\mu_r = 10, \alpha = 1.5$, $U_E = 0, , \phi_{oc} = 0.75, \beta = 2$. and the peripheral region(right panels) with other parameters $Q = 4$, *k=0.8* $\mu_r = 0.1, \alpha = 1.5, \beta = 2$, $U_E = 0, , \phi_{oc} = 0.75$. The dashed line indicates the interface region.

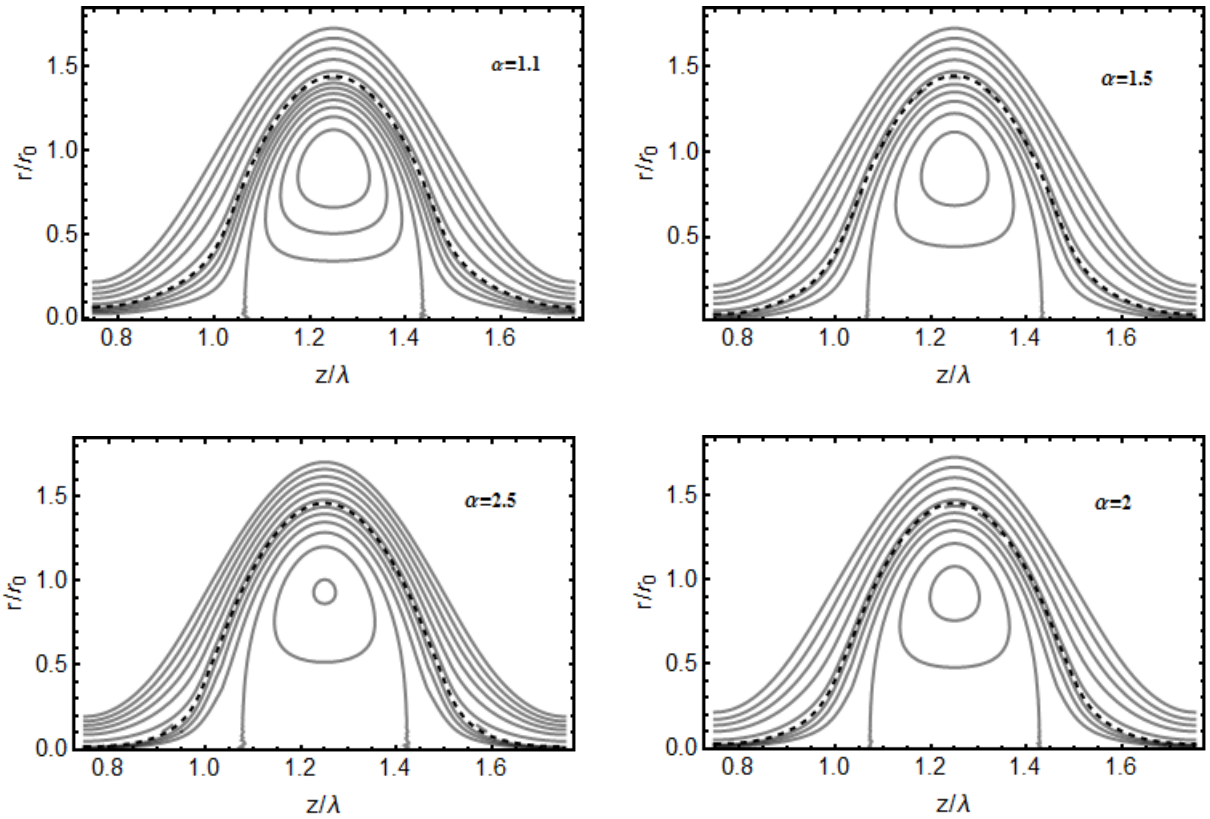

Fig. 6. Trapping phenomena for different values of α when $Q = 0,\ \mu_r = 10, \beta = 2, k = 0.4, U_E = 0, \phi_{oc} = 0.75$.

The identification of plausible value of ϕ_{oc} and $Q/Q_{\Delta p=0}$ is carried out first by obtaining a trial subregion in the domain $\left(0 \leq Q/Q_{\Delta p=0} \leq 1\right);\ \ (0 \leq \phi_{oc} \leq 1)$ where the stream function ψ changes its sign and then employing a root-finding algorithm to exactly pinpoint the value of ϕ_{oc} and ψ at which such a transition occurs [31].

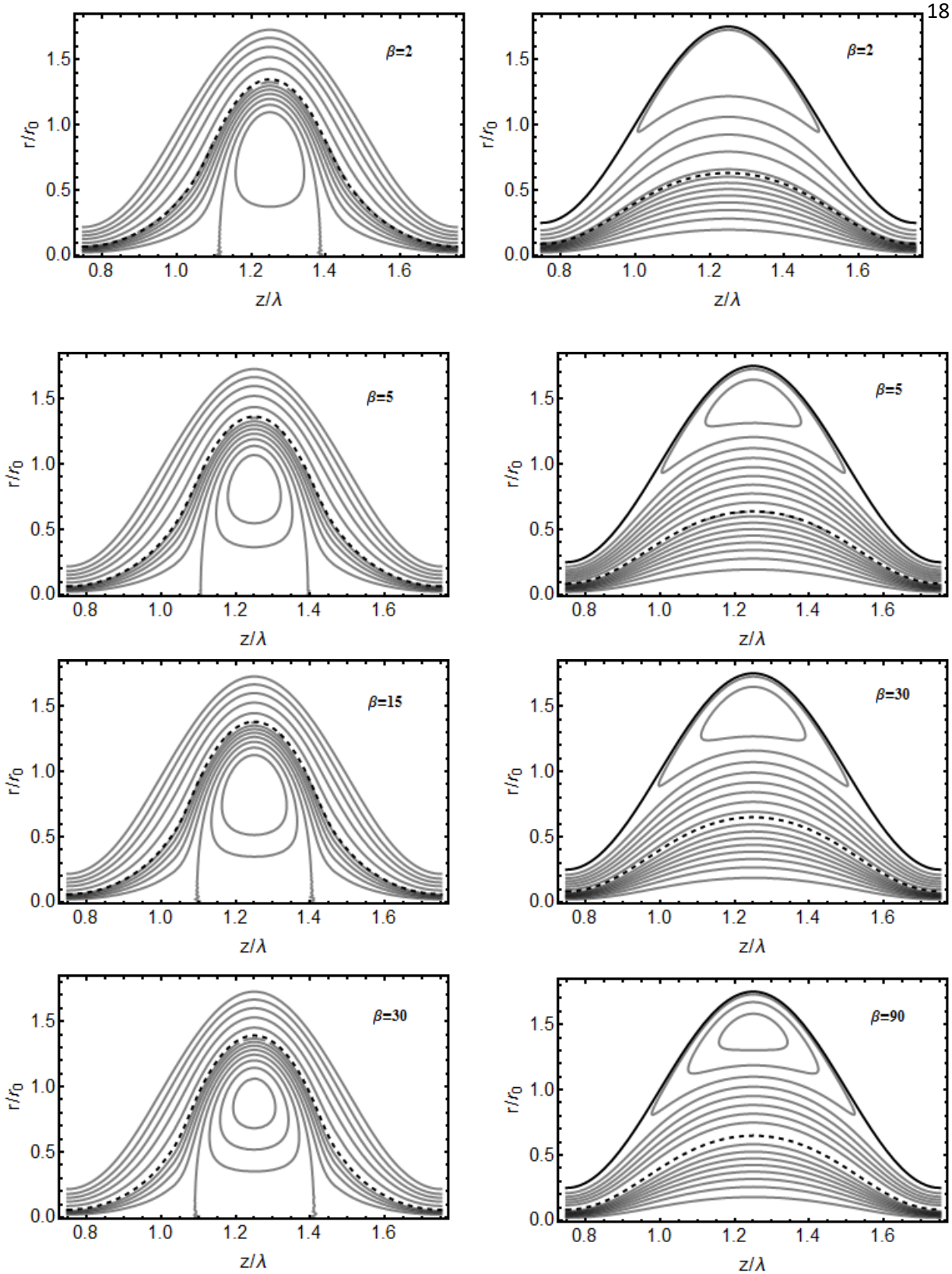

Fig. 7. The streamline plots showing the trapping inside the core region with other parameters $\boldsymbol{Q = 0}$, k=0.4, $\mu_r = \mathbf{1}, \boldsymbol{\alpha = 1.5}$, $\boldsymbol{\beta = 2}$, , $\boldsymbol{\phi_{oc} = 0.75}$ *(left side)* and peripheral region with other parameters $\boldsymbol{Q = 4}$, k=0.4 $\mu_r = \mathbf{1}, \boldsymbol{\alpha = 1.5}$, $\boldsymbol{\beta = 2}$, , $\boldsymbol{\phi_{oc} = 0.75}$ *(right side).* The dashed line presents the interface region.

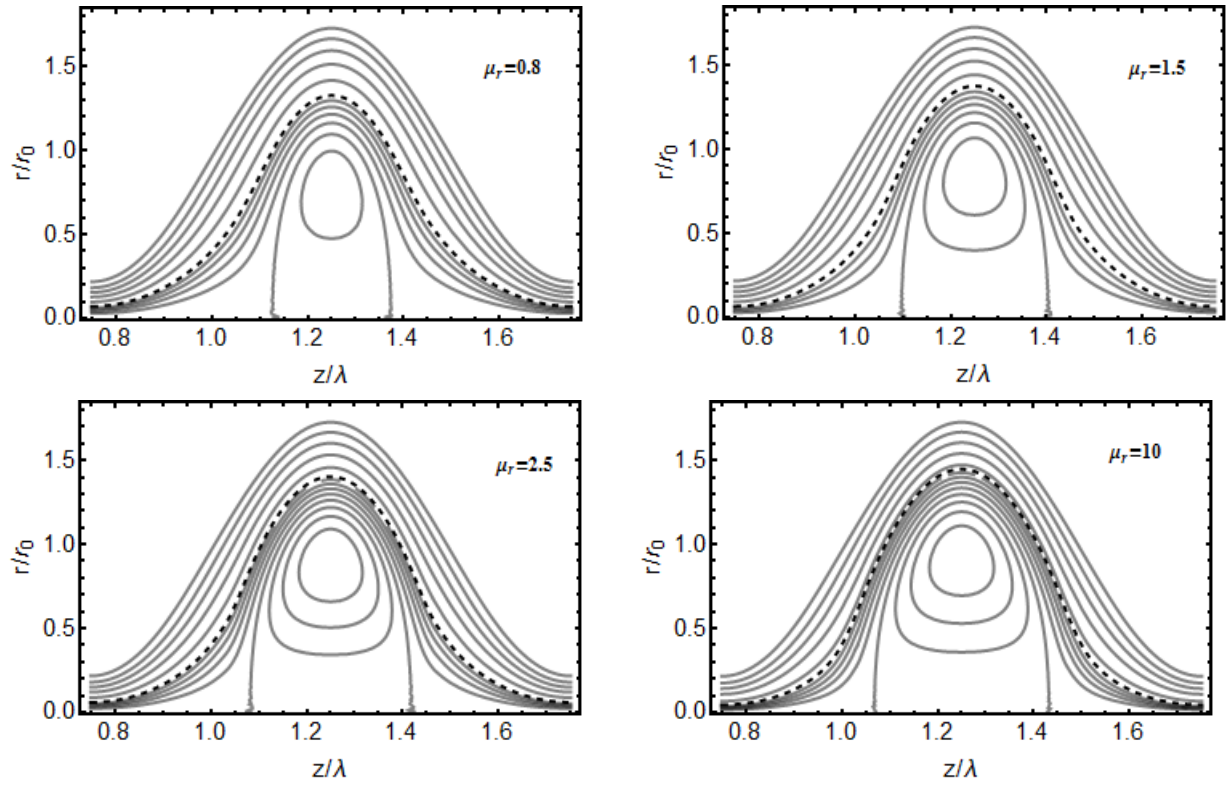

Fig. 8. Trapping phenomena for different values of μ_r and the values of other parameters are $Q = 0$, $2, \alpha = 1.5, U_E = 0, \phi_{oc} = 0.75, , \beta = 2, k = 0.4$.

Two distinct regions can be readily identified for each figure. One below a specific curve and the other one above it. The region of trapping comprises of the zone that lies above a specific curve in the ϕ_{oc} - $Q/Q_{\Delta p=0}$ plane. **Fig. 9** shows the effect of the electro-osmotic slip velocity on the trapping region. It is observed that trapping region reduces with increasing the electro-osmotic slip velocity, power-law index α and the viscosity ratio μ_r. In contrast, it increases with increasing the Ellis parameter β.

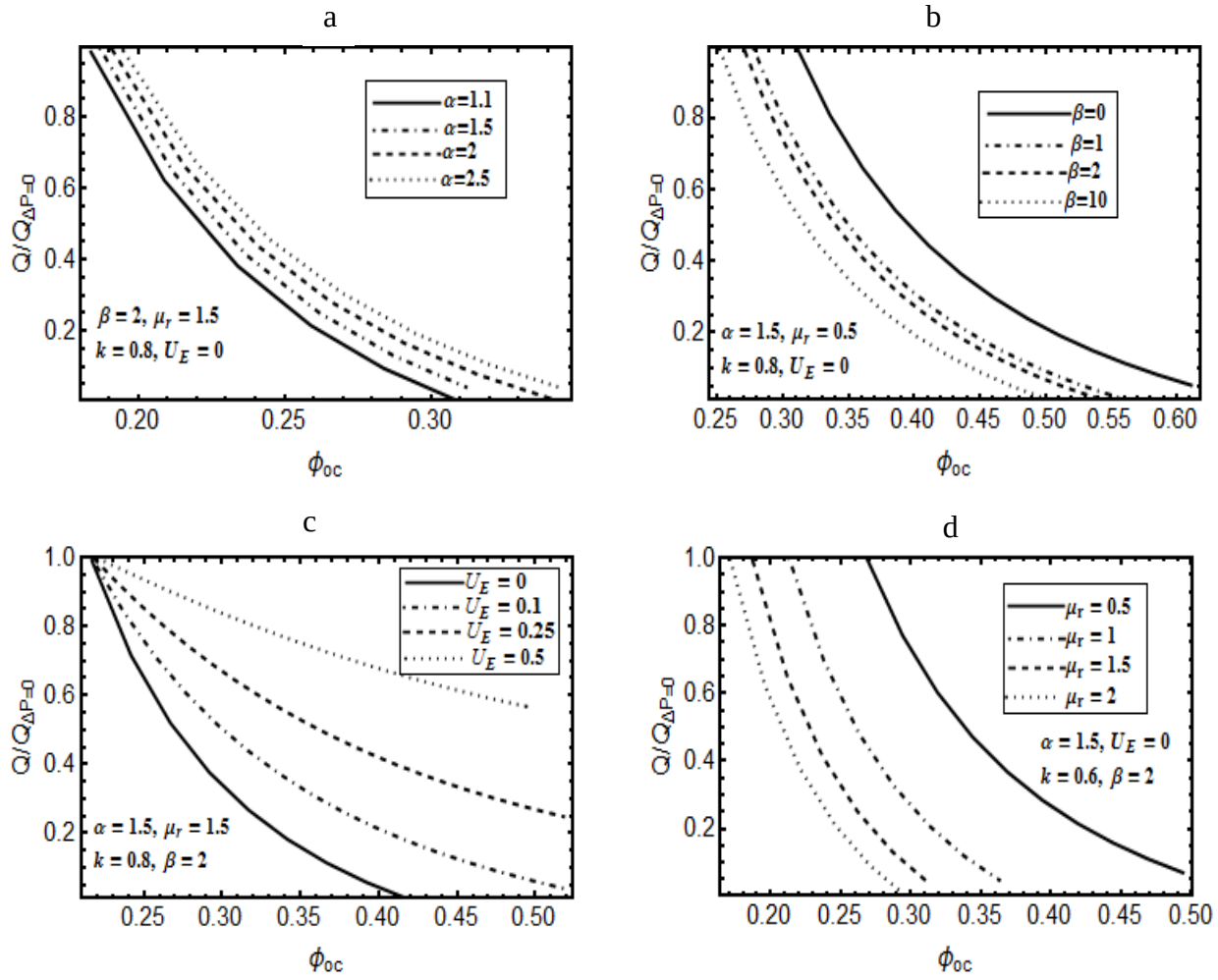

Fig. 9. Showing the trapping limits for different values of parameters (a) show that the variation of $\boldsymbol{\alpha}$ (b) show that the variation of $\boldsymbol{\beta}$ (c) show that the variation of electrokinetic slip velocity (d) show that the variation viscosity ratio.

Reflux is the process in which the fluid moves in backward direction in a complete wave cycle due to the unfavorable pressure gradient across the flow geometry or by the opposite movement of a fluid element inside the tube [31]. It is anticipated that the reflux phenomenon in both regions depends strongly on the involved parameters. According to Shapiro *et al.* [1], the amount of reflux can be estimated through the quantity $(Q - Q_\psi)/Q$ during one wave cycle, where Q_ψ is defined as [4]:

$$Q_\psi = 2\psi + \int_0^1 r^2 \, dr. \tag{47}$$

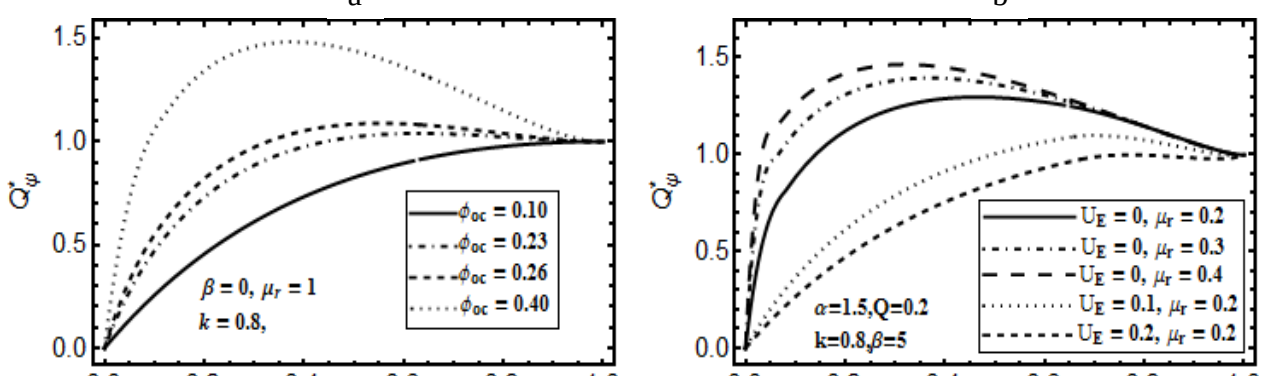

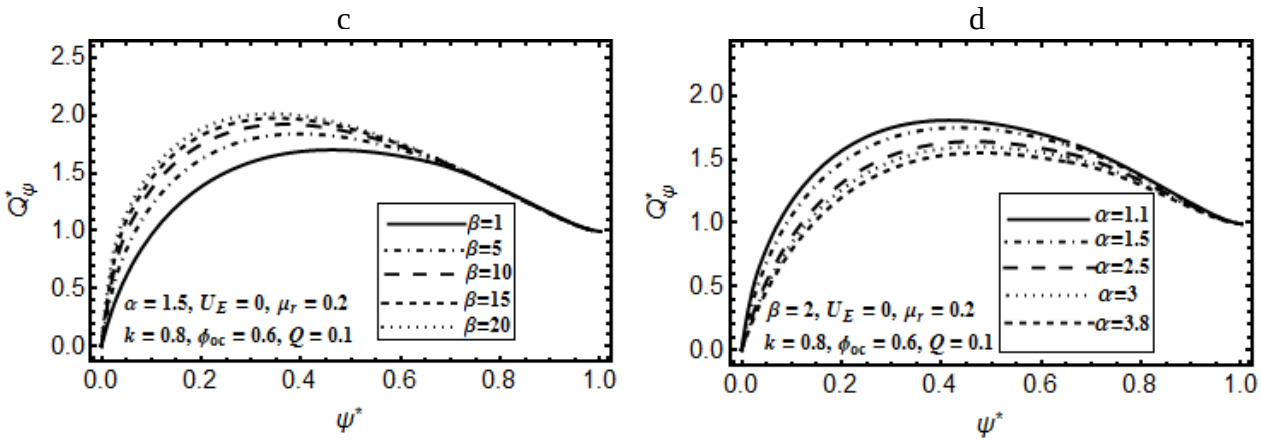

Fig. 10. Show that the reflux phenomena (a) for Newtonian fluids (b) for different values of electrokinetic slip velocity and viscosity ratio. (c) for different values of Ellis model parameter $\boldsymbol{\beta}$ (d) for different values of Ellis index parameter $\boldsymbol{\alpha}$.

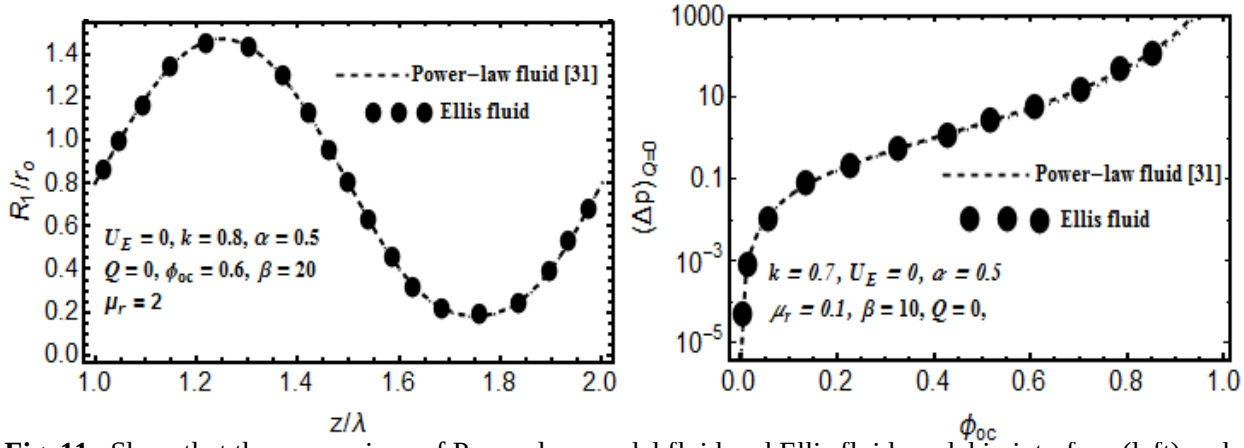

Fig. 11. Show that the comparison of Power-law model fluid and Ellis fluid model in interface (left) and pressure (right).

The above expression emerges by transforming the following expression from the fixed frame to the wave frame and taking the average over one period of the wave:

$$Q_{\psi'} = 2\int_0^{r(\psi',z)} r\, w\, dr, \tag{48}$$

In (48) $Q_{\psi'}$ is the average volume flow rate between the axis of the tube and a streamline ψ'=constant in the fixed frame. Since the quantity Q_ψ/Q varies between 0 to 1 therefore the

quantity $(Q - Q_\psi)/Q$ must vary from 1 to 0. However, under certain conditions it may happen that for some values of ψ' the quantity Q_ψ/Q exceeds unity, or, the quantity $(Q - Q_\psi)/Q < 0$ which is an indicator that there is some sort of backward motion or reflux occurring within the flow domain. **Fig. 10** shows that reflux can avoided by increasing the electro-osmotic slip velocity U_E and the fluid power-law index α. In contrast, reflux is enhanced with an increase in both the viscosity ratio μ_r and the Ellis parameter β.

Finally, we demonstrate the generality of the present analysis in comparison to the previously published results. To this end, we have shown in **Fig.11** that the results for the situation when the fluid in the core region is characterized by power-law model can be deduced from the present analysis by proper selection of the Ellis parameter α and β. Obviously, the present results also contract to the results for the case when the fluid in the inner region obeys the Newtonian constitutive law by setting $\alpha = 1,\ \beta = 0$.

5. Conclusions

In the present article, an analysis is presented for peristaltic motion of two immiscible fluids in a tubular confinement under electro-osmotic body force. The core region fluid is assumed to obey the Ellis constitutive equation whereas the peripheral region fluid is characterized by the Newtonian model. The stream function for each region is derived for the case when the shape of the interface is not known a priori. The important phenomena of pumping, trapping and reflux are discussed in detail. It is found that the maximum pressure against which peristalsis has to work as a positive displacement pump can be reduced by choosing small values of the Ellis model parameters α and β. Further, trapping and reflux phenomena can be avoided by enhancing the electro-osmotic slip and shear-thinning effects. In blood vessels, trapping is undesirable owing to its role is the formation of thrombosis of blood. Similarly, it may also trigger undesired chemical reactions in reactive fluids. The reflux in the context of biological fluid transport is also undesirable since it contributes to the migration of micro-organism in the opposite direction to the peristaltic wave motion. Moreover, in the magnitude of dimensionless pressure produced by the wavy wall motion of the tube is linked with the efficiency of the pumping and therefore needs to be reduced. Our results suggest the following possible remedies to avoid trapping and reflux and to reduce the

pressure evolved by the wall movement. The first option is the imposition of the electro-osmotic slip velocity which has already been proposed by previous researchers [19, 25 - 31]. This solution is universal in the sense that it minimizes all three of the above-mentioned phenomena. The other possible way is to *enhance the shear-thinning nature* of the fluid to be transported. Similarly, the reduction in pressure and reflux can also be achieved by properly tuning the rheological characteristics of the fluid controlled by the parameter τ_0. However, this will happen at the cost of an increase in the trapping phenomenon.

References

[1] A. H. Shapiro, M. Y. Jaffrin, S. L. Weinberg, Peristaltic pumping with long wavelength at low Reynolds number, *Journal of Fluid Mechanics*, 37, 799-825 (1969).

[2] K. K. Raju, R. Devanathan, Peristaltic motion of a non-Newtonian fluid, *Rheologica Acta*, 11, 170-178 (1972).

[3] A. M. Provost, W. H. Schwarz, A theoretical study of viscous effects in peristaltic pumping, *Journal of Fluid Mechanics*, 279, 177-195 (1994).

[4] A. R. Rao, M. Mishra, Peristaltic transport of a power-law fluid in a porous tube, *Journal of Non-Newtonian Fluid Mechanics*, 121, 163-174 (2004).

[5] T. Hayat, Q. Hussain, N. Ali, Influence of partial slip on the peristaltic flow in a porous medium, *Physica A: Statistical Mechanics and Applications*, 387, 3399– 3409 (2008).

[6] T. Hayat, N. Saleem, N. Ali, Effect of induced magnetic field on peristaltic transport of a Carreau fluid, *Communication in Nonlinear Science and Numerical Simulation*, 15, 2407–2423 (2010).

[7] A. R. Rao, M. Mishra, Nonlinear and curvature effects on peristaltic flow of a viscous fluid in an asymmetric channel, *Acta Mechanica*, 168, 35-59 (2004).

[8] S. Usha, A. R. Rao, Effect of curvature and inertia on the peristaltic transport in a two-fluid system, *Int. J. Engineering Science*, 38, 1355-1375 (2000).

[9] T. Hayat, S. Farooq, B. Ahmad, A. Alsaedi, Characteristics of convective heat transfer in the MHD peristalsis of Carreau fluid with Joule heating, *AIP Advances*, 6, 045302 (2016).

[10] J. C. Misra, B. Mallick, A. Sinha, Heat and mass transfer in asymmetric channels during peristaltic transport of an MHD fluid having temperature-dependent properties, *Alexandria Engineering Journal*, 57, 391-406 (2018).

[11] N. Ali, M. Sajid, T. Javed, Z. Abbas, Heat transfer analysis of peristaltic flow in a curved channel, *International Journal of Heat and Mass Transfer*, 53, 3319-3325 (2010).

[12] D. Takagi, N. J. Balmforth, Peristaltic pumping of viscous fluid in an elastic tube, *Journal of Fluid Mechanics*, 672, 196-218 (2011).

[13] D. Takagi, N. J. Balmforth, Peristaltic pumping of rigid objects in an elastic tube, *Journal of Fluid Mechanics*, 672, 219-244 (2011).

[14] N. Ali, K. Javid, M. Sajid, Simulations of peristaltic slip-flow of hydromagnetic bio-fluid in a curved channel, *AIP Advances* 6, 025111 (2016).

[15] N. Ali, K. Javid, M. Sajid, A. Zaman, T. Hayat, Numerical simulations of Oldroyd 8-constant fluid flow and heat transfer in a curved channel, *International Journal of Heat and Mass Transfer*, 94, 500–508 (2016).

[16] A. Tanveer, T. Hayat, F. Alsaadi, A. Alsaedi, Mixed convection peristaltic flow of Eyring-Powell nanofluid in a curved channel with compliant walls, *Computers in Biology and Medicine*, 82, 71-79 (2017).

[17] T. Hayat, N. Ali, Z. Abbas, Peristaltic flow of a micropolar fluid in a channel with different wave forms, *Physics Letters A*, 370, 331-344 (2007).

[18] A. I. Dobrolyubovn, G. Douchyz, Peristaltic transport as the travelling deformation waves, *J. Theoretical Biology*, 219, 55–61 (2002).

[19] S. Chakraborty, Augmentation of peristaltic microflows through electro-osmotic mechanisms, *Journal of Physics D: Applied Physics*, 39, 5356-5363 (2006).

[20] M. Zhao, S. Wang, S. Wei, Transient electro-osmotic flow of Oldroyd-B fluids in a straight pipe of circular cross section, *Journal Non-Newtonian Fluid Mechanics*, 201, 135-139 (2013).

[21] C. Zhao, C. Yang, Electro-osmotic flows of non-Newtonian power-law fluids in a cylindrical microchannel, *Electrophoresis*, 34, 662-667 (2013).

[22] D. A. Saville, Electro-kinetic effects with small particles, *Annual Review Fluid Mechanics*, 9, 321–337 (1977).

[23] A. M. Afonso, M. A. Alves, F. T. Pinho, Analytical solution of mixed electro-osmotic pressure driven flows of viscoelastic fluids in microchannels, *Journal Non-Newtonian Fluid Mechanics*, 159, 50-63 (2009).

[24] A. M. Afonso, M. A. Alves, F. T. Phino, Analytical solution of two-fluid electro-osmotic flow of viscoelastic fluid, *Journal Colloid and Interface Science,* 395, 277-286 (2013).

[25] S. Dhinakaran, A. M. Afonso, M. A. Alves, F. T. Phino, Steady viscoelastic fluid flow between parallel plates under electro-osmotic forces, *Journal Colloid and Interface Science,* 344, 513-520 (2010).

[26] L. L. Ferras, A. M. Afonso, M. A. Alves, F. T. Phino, J. M. Noberga, Analytical and numerical study of the electro-osmotic annular flow of viscoelastic fluid, *Journal Colloid and Interface Science,* 420, 152-157 (2014).

[27] S. Das, S. Chakraborty, Analytical solution for velocity, temperature and concentration distribution in electro-osmotic microchannel flows of a Non-Newtonian biofluid, *Analytica Chimica Acta*, 559, 15-24 (2006).

[28] D. Tripathi, S. Bhushan, O. Anwar Bég, Transverse magnetic field driven modification in unsteady peristaltic transport with electrical double layer effects, *Colloids and Surfaces A: Physicochem. Engineering Aspects* 506, 32–39 (2016).

[29] D. Tripathi, A. Sharma, O. Anwar Bég, Joule heating and buoyancy effects in electro-osmotic peristaltic transport of aqueous nanofluids through a microchannel with complex wave propagation, *Advanced Powder Technology*, 29, 639-653 (2018).

[30] J. Prakash, D. Tripathi, Electroosmotic flow of Williamson ionic nanoliquids in a tapered microfluidic channel in presence of thermal radiation and peristalsis, *Journal of Molecular Liquids*, 256, 352-371 (2018).

[31] P. Goswami, J. Chakraborty, A. Bandopadhyay, S. Chakraborty, Electrokinetically modulated peristaltic transport of power-law fluids, *Microvascular Research*, 103 41-54(2016).

[32] N. Ali, A. Abbasi, I. Ahmed, Channel flow of Ellis fluid due to peristalsis, *AIP Advances*, 5, 097214 (2015).

[33] J. S. Goud, R. H. Reddy, Peristaltic motion of an Ellis fluid model in a vertical uniform tube with wall properties, *International Journal of Civil Engineering and Technology*, 9, 847–856 (2018).

[34] R. J. Hunter, *Zeta Potential in Colloid Sciences: Principles and Applications*. Academic Press, London (1981).